

# COMMUTER AIRCRAFT AERODYNAMIC DESIGN: WIND-TUNNEL TESTS AND CFD ANALYSIS

**Fabrizio Nicolosi\***, **Salvatore Corcione\***, **Pierluigi Della Vecchia\***  
**\*Dept. of Industrial Engineering - University of Naples "Federico II"**  
*fabrizio.nicolosi@unina.it*

**Keywords:** *Wind-tunnel tests, CFD, Commuter Aircraft*

## Abstract

*The paper presents wind-tunnel tests and CFD numerical aerodynamic analysis of Tecnam P2012 Traveller aircraft. An extensive wind tunnel tests campaign of several different modular aircraft configurations analyzed has been performed on a scaled model in order to experimentally estimate both longitudinal and lateral-directional stability, control derivatives, and to improve the aircraft aerodynamic performances. Simultaneously numerical investigations through a CFD software has been performed, both at wind-tunnel tests Reynolds number ( $Re=0.6$  millions) and at free flight Reynolds number of the full scale aircraft ( $Re=4$  or  $9$  millions). Finally results are compared showing a good agreement in the lift and pitching moment coefficient both with and without control surfaces or flap deflections, and an underestimation of drag coefficient in the CFD numerical analysis. Horizontal tail positions are also tested in wind-tunnel and compared to CFD analysis highlighting how an accurate design leads to improvement both in stability and control. Results will be very useful in the final design of the aircraft and to perform dynamic simulations.*

## Nomenclature

AR aspect ratio  
ADAG Aircraft Design and AeroflightDynamics Group  
 $b$  wing span  
 $b_H$  horizontal tail span  
 $b_V$  vertical tail span

$\bar{c}$  mean aerodynamic chord  
DII Department of Industrial Engineering  
 $h_F$  fuselage height  
 $l_F$  fuselage length  
 $\lambda$  taper ratio  
 $S$  wing surface  
 $S_H$  horizontal tail surface  
 $S_V$  vertical tail surface  
 $w_F$  fuselage span

### Aerodynamic coefficients

$C_D$  drag coefficient  
 $C_L$  lift coefficient  
 $C_{L0}$  alpha zero lift coefficient  
 $C_{L\alpha}$  lift coefficient derivative  
 $C_{roll}$  rolling moment coefficient  
 $C_{roll\beta}$  rolling moment derivative  
 $C_{M0}$  pitching moment coefficient at  $\alpha = 0$   
 $C_{M\alpha}$  pitch stability derivative  
 $C_N$  yawing moment coefficient  
 $C_{N\beta}$  yawing moment derivative  
 $C_{Y\beta}$  sideforce derivative

### Capital letters

B body or fuselage  
V vertical tailplane  
WWB wing winglet body  
WWBN wing winglet body nacelle  
WWBNHV wing winglet body nacelle + horizontal and vertical tail

## 1 Introduction

The Tecnam P2012 Traveller is a twin engine eleven seats aircraft designed by Prof. Luigi Pascale at Tecnam Aircraft Industries. The aerodynamic design of the aircraft has also been

accomplished through the collaboration with the Aircraft Design Group of Department of Industrial Engineering (DII), University of Naples “Federico II”. In the last 20 years the authors have gained experiences in the design of very light and CS-23 certified aircraft [1]-[6]. Several numerical methodologies and experimental technologies (wind-tunnel tests and flight tests) useful during preliminary aircraft design have been developed at the ADAG and presented in [2]. A three lifting surface radio-model design and flight tests is described in ref. [3]. In ref. [4] and [5] the design of a low-costs STOL ultra-light aircraft characterized by application of composite materials has been carried out and subsequently tested in wind-tunnel facility.

In ref. [6]-[7], the design, numerical aerodynamic analyses, wind-tunnel tests, flight tests, certification and in-flight parameter estimation have been carried out on the Tecnam P2006T aircraft (twin engine CS-23 certified).

Since 2011 Tecnam Aircraft Industries and researchers at DII are deeply involved in the design of a new 11 seats commuter aircraft, the P2012 Traveller. Design guidelines, specific market opportunities and preliminary wind-tunnel tests have been outlined by the authors in ref.[9]-[13]. In the last year an interesting collaborative aircraft design between ADAG and University of Stockholm have been carried out applied to an example of a 16 seat turboprop aircraft [14].

During last 3 years, the authors have massively intensified the use of CFD Navier-Stokes aerodynamic analyses [15]-[19]. Thanks to availability of the University's computing grid infrastructure ScoPE [20] to perform parallel computing simulations and the commercial CAE package Star-CCM+ [21], Navier-Stokes aerodynamic analyses on complete aircraft configurations in a relative short amount of time have been made possible. The present work aims to provide a synthesis and comparison of the main experimental (wind-tunnel tests) and numerical (CFD Navier-Stokes) aerodynamic analyses on the Tecnam P2012 Traveller aircraft. Section 1.1 describes the aircraft main features and geometrical data. Section 2 presents the main wind-tunnel results and in

section 3 the Navier-Stokes aerodynamic analyses are compared to these tests.

### 1.1 The Tecnam P2012 Aircraft

Tecnam P2012 Traveller is a twin engine, 11 seat aircraft, high-wing and body mounted horizontal tail. Design specifications have led to a fixed landing gear, high cabin volume and short take-off and landing distances.

The aircraft is powered by two Lycoming piston TEO-540-A1A engines. The Tecnam P2012 Traveller will be used both as a passenger airplane but has been designed to be a very versatile and flexible aerial platform, offering multi-role opportunities including VIP travel, cargo shipping, parachuting, medevac services and more besides (see [9]- [13]). Table 1 shows some main external dimensions of the P2012 Traveller, while Table 2 summarizes some of estimated aircraft flight performance.

Symbol	Value
S	25.4 m <sup>2</sup> (268.2 fts <sup>2</sup> )
b	14.0 m (45.9 fts)
AR	7.72
$\bar{c}$	1.87 m (6.14 fts)
$\lambda$	0.73
S <sub>H</sub>	6.10 m <sup>2</sup> (65.7 fts <sup>2</sup> )
b <sub>H</sub>	5.70 m (18.7 fts)
S <sub>V</sub>	3.52 m <sup>2</sup> (37.9 fts <sup>2</sup> )
b <sub>V</sub>	2.53 m (8.3 fts)
l <sub>F</sub>	11.59 m (38.0 fts)
h <sub>F</sub>	1.60 m (5.25 fts)
w <sub>F</sub>	1.60 m (5.25 fts)

Table 1 – P2012 Traveller geometrical characteristics

Estimated Performance	Value
Rate of Climb (AEO)	8.1 m/s (1600 fts/min)
Rate of Climb (OEI)	2.0 m/s (400 fts/min)
Max. Speed	192 kts @s.l., 205 kts @6000 fts, 209 kts @8000 fts
Cruise Speed (75% Power)	170 kts @s.l., 181 kts @6000 fts, 185 kts @8000 fts
Stall Speed (T.O. Configuration)	33 m/s (65 kts)
Stall Speed (Full Flap)	31 m/s (60 kts)
Minimum Control Speed (VMC)	38 m/s (74 kts)
Take Off Distance (15 m)	1840 fts
Landing Distance (15 m)	1660 fts
Accelerate Stop Distance	1870 fts
Range (Max. Payload, 65% Power)	711 Km (384 nmi)
Range (Max. Fuel, 65% Power)	1226 Km (662 nmi)

Table 2 – P2012 Traveller estimated performances

## 2 Wind-tunnel Tests

The experimental tests campaign has been performed in the main subsonic wind tunnel facility of the DII of the University of Naples.

The tested model is a 1:8.75 aircraft scale model. Main dimensions of the tested model are summarized in Table 3, where it is also illustrated the chosen position of the reference point for the estimation of the aerodynamic moment. This point represents a reasonable position for the aircraft center of gravity. Figure 1 shows the complete aircraft in the wind tunnel section.

Symbol	
b	1.60 m
S	0.33 m <sup>2</sup>
l <sub>f</sub>	1.34 m
$\bar{c}$	0.214 m
$x_{cg}/\bar{c}, z_{cg}/\bar{c}$	0.25

Table 3 – Scaled model (1:8.75) main external dimensions

The measurements of the aerodynamic forces and moments acting on the model have been made possible through the use of internal strain-gage balances. The strain gage balances have been subjected to a calibration procedure for the right estimation of the aerodynamic forces and moments.



Figure 1 – P2012 1:8.75 scale model, in the wind tunnel facility of DII.

All tests have been performed at the maximum available wind speed (about 38-40m/s) with a Reynolds number of about 0.6 million (referred to the mean aerodynamic chord, see Table 3), therefore, to avoid aerodynamic phenomena

dealing with the low Reynolds number effects (such as laminar bubbles), transitional strips have been placed on all components of the aircraft in order to promote the transition of the flow. The right thickness and the right position of the transitional strips has been estimated by tests of flow visualization through the use of coloured oil (transitional strips have been placed at 5% of local chord, both on the lower and upper surfaces, of all components and have a thickness of about 0.5mm), as shown in Figure 2.

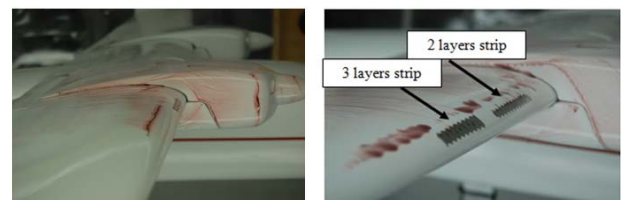


Figure 2 – Example of flow visualization of laminar bubble on the wing upper surface and the effects of the transitional strips thickness, Re=0.6e6 and  $\alpha=4^\circ$ .

The figure shows an example of flow visualization of laminar separation bubble on the wing upper surface and the transition promoted by the transitional strips, at Re=0.6e6 and  $\alpha=4^\circ$ .

To take into account the effect of the wind tunnel walls all the required corrections have been applied to the experimental results as suggested by Pope [11].

### 2.1 Longitudinal wind-tunnel tests

Tests have been performed on the complete aircraft model and on several configurations with only some components in order to measure the complete aircraft lift, stability and control characteristics and also to estimate the contribution of each aircraft component. An experimental investigation about the best vertical positioning of the horizontal tail will be also presented.

#### 2.1.1 Lift and longitudinal stability breakdown, flap effect and longitudinal control

This section shows the measured lift and pitching moment coefficient and also highlights how several aircraft component contribute to these aerodynamic characteristics. The complete aircraft shows a lift curve slope of about

0.0911deg<sup>-1</sup> and a pitching moment derivatives respect to the angle of attack of about -0.0237deg<sup>-1</sup>. The fuselage produces a forward shift of the aerodynamic center of about 12% while the two nacelles lead to a neutral effect in lift curve slope and a furthermore forward shift of the aerodynamic center of about 3.5% (see Figure 3 and Figure 4).

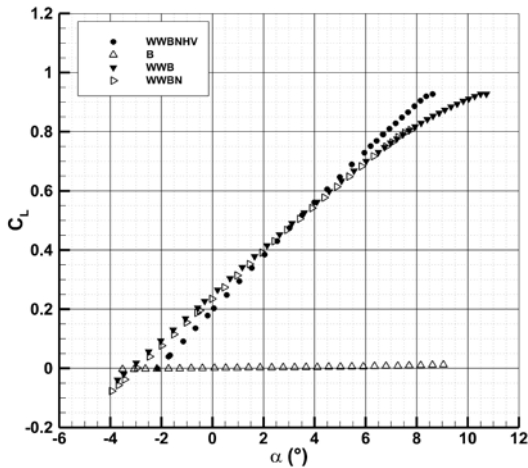


Figure 3 – Aircraft lift coefficient breakdown, Re=0.6e6

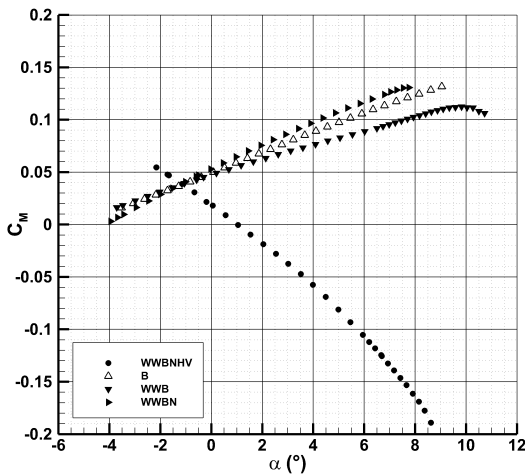


Figure 4 – Aircraft pitching moment coefficient breakdown, Re=0.6e6

Two flap deflections have been investigated; 15° (typical of take-off phase) and full flap 40° (typical of landing condition). Figure 5 shows the typical flap effect on the lift curve. The lift curve slope is slightly affected (only at flap 40 deg.) while a  $\Delta C_{L_{OF}}$  of about 0.24 and 0.78, for the take-off and landing conditions respectively has been measured.

Figure 6 shows the flap effect on the longitudinal stability. It can be noticed that the neutral point location moves forward of about 3%  $\bar{c}$  in the full flap condition, as matter of fact

the neutral point moves from the 48%  $\bar{c}$ , in flap up and take-off condition, to the 45%  $\bar{c}$  with a full flap deflection (at alpha=0 deg.,  $C_L = 0.8-1.0$ ). This is mainly due to the wing wake interaction with the horizontal tailplane at low angles of attack (alpha body = 0 deg.). As it can be noticed from figure 6, at higher angles of attack and flap 40 deg. , the aircraft stability increases again (the wing wake moves up and increases its distance to the horizontal tailplane). These aerodynamic phenomena will be better explained in the next section dealing with the horizontal tail positioning.

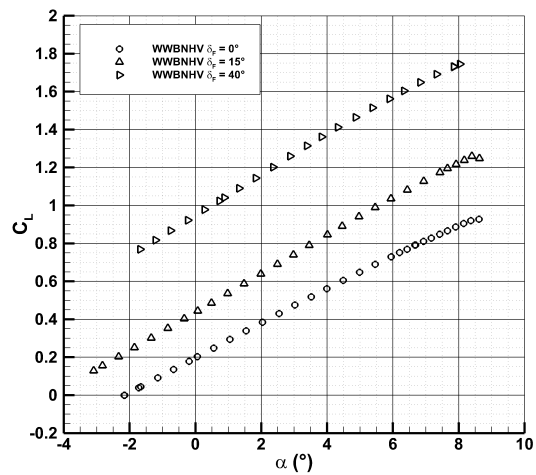


Figure 5 – Flap deflection,  $C_L$  vs.  $\alpha$ , Re=0.6e6

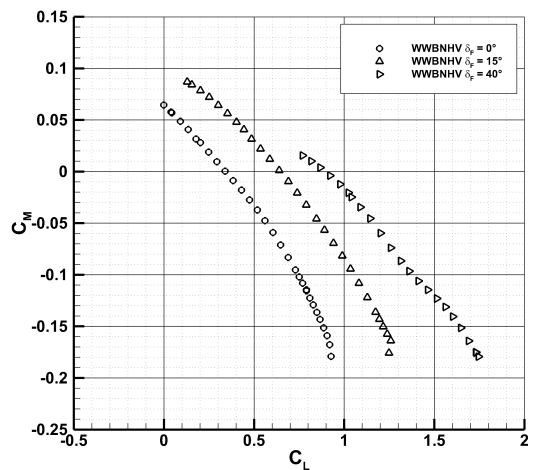


Figure 6 – Flap deflection,  $C_M$  vs.  $C_L$ , Re=0.6e6

Experimental investigations have been performed also in order to evaluate the aircraft trim capabilities. The trim analysis has been performed both in flap up and landing condition. The most forward position of the

aircraft centre of gravity (based on preliminary aircraft weight and balance calculations) has been chosen ( $18\% \bar{c}$ ). Figure 7 shows the trim analysis in full flap condition. The horizontal tail incidence angle for all tests performed is  $0^\circ$ . The final incidence for the horizontal stabilizer to be chosen for the full scale aircraft maybe will be slightly negative (i.e.  $-1$  deg), to increase pitch-up equilibrium and trim capabilities (useful for flight trim in landing, but also for take-off rotation phase).

*2.1.2 Experimental investigation about the vertical positioning of the horizontal tail*

It is well known that the horizontal tail vertical position can lead to aerodynamic problems or different stability characteristics in relation to its distance from wing wake. As usually carefully considered in preliminary design, the wing downwash at tail is dependent from the vertical distance from the wing wake, as can be easily estimated through some very simple semi-empirical procedure, see [12].

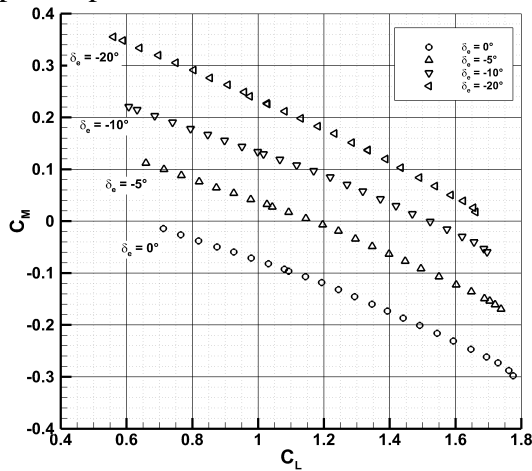


Figure 7 – Trim analysis, full flap,  $x_{cg}$  at 18%,  $C_M$  vs.  $C_L$ ,  $Re=0.6e6$ .

Horizontal tailplane and wing wake interaction can lead not only to longitudinal stability reduction (for the reduced dynamic pressure at tail and downwash), but also a possible dangerous condition, such as stick buffeting and structural fatigue for the horizontal tailplane structure. Usually some semi-empirical method like [12] can be also used to check the chosen position and to avoid these phenomena. Therefore one of the main goals of the preliminary design phase has been the identification of the best vertical positioning for

the horizontal tail plane, in order to guarantee the minimum interference of the wing wake on the horizontal tail plane leading to the best longitudinal stability and avoiding both buffeting problems due to the wing wake interaction with the horizontal tail plane and reduction of the longitudinal stability due to the loss in the dynamic pressure for the horizontal tail plane.

The original P2012 configuration layout provides for a body mounted horizontal tail with a symmetrical fuselage tailcone. This position for the horizontal tail plane could be interested by the wing wake in full flap and low angles of attack condition; this and also considering that many similar aircraft such as the Cessna Caravan or the Britten Norman.

Tested tail positions are those previously illustrated in Figure 8.



Figure 8 – Tested positions of the horizontal tail

In order to evaluate the effect of the flap deflection on the horizontal tail, three flap conditions have been tested: flap up (cruise condition), flap  $15^\circ$  (take-off condition) and full flap  $40^\circ$  (landing condition).

Results of those tests have highlighted how the longitudinal stability is variable with the lift coefficient range, and it is affected by the horizontal tail position especially for the flapped configurations, where the wing wake interaction with the tail surface became stronger. Table 4 shows the neutral point location, in percentage of the mean aerodynamic chord, for typical lift conditions.

Figure 9 clearly shows how in the flap up condition the longitudinal stability gradually decreases as well as the horizontal tail approaches the wing trailing edge (from POS.A to POS.C), since the downwash became stronger and the wing wake reduces the dynamic pressure acting on the tail, conversely in full flap condition (see Figure 10) at low attitude POS.A is critical for stability for the same reasons.

The POS.C can be a critical position for the horizontal tailplane since the tail surface is seriously interested by the wing wake at high speed (cruise condition) with high risks of possible stick buffeting and structural fatigue for the horizontal tailplane structure.

Table 4 shows how in the take-off flap condition the POS.B and POS.C are characterised by an area of sensible reduction of the stability due to the strong interaction of the wing wake with the tail surface. The neutral point moves forward from the 51% to the 44% along the mean aerodynamic chord ( $C_L = 0.4-0.8$ ). Table 4 also illustrates how the POS.A, in the full flap configuration (landing condition), show an area of a lower longitudinal stability at low angles of attack that are in any case not typical condition for the aircraft landing phase.

CONFIGURATION	$N_0$ (% $\bar{c}$ )		
	POS. A	POS. B	POS. C
FLAP = 0°, $C_L = 0.5$	46.3	45.5	42.3
FLAP = 15°, $C_L = 0.8$	51.0	43.4	44.4
FLAP = 40°, $C_L = 1.3$	48.0	47.2	51.3

Table 4 - Effect of vertical position of the horizontal plane

This experimental investigation has led to identify the POS. A as the best position for the horizontal tail plane among all those tested.

### 2 Lateral-Directional wind-tunnel tests

Complete aircraft configuration, isolated vertical tail and body have been tested in order to estimate the contribution to directional and lateral stability of each aircraft component. Figure 11 shows the yawing moment coefficient variation respect to the sideslip angle of the complete aircraft, the isolated vertical tail and the isolated fuselage. As it can be seen in Figure 11 the vertical tail effectiveness is increased by aircraft components mutual effects. In fact the stabilizing effect of the vertical tailplane when considered mounted on the fuselage and with the horizontal tailplane, is about 25% to 30% higher.

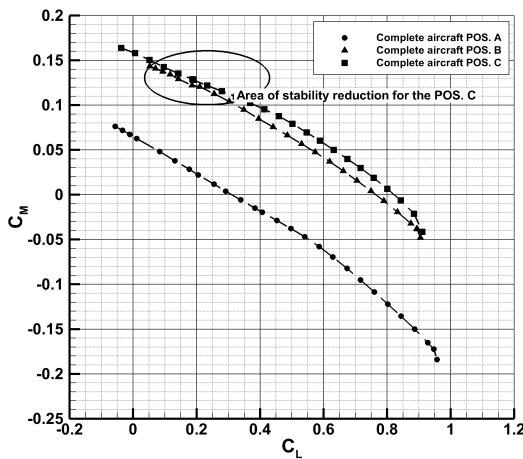


Figure 9: Effect of vertical positioning of the horizontal tail, pitching moment coefficient, Flap = 0°,  $x_{cg}/c=0.25$   $z_{cg}/c = 0.25$   $i_{to} = 0^\circ$

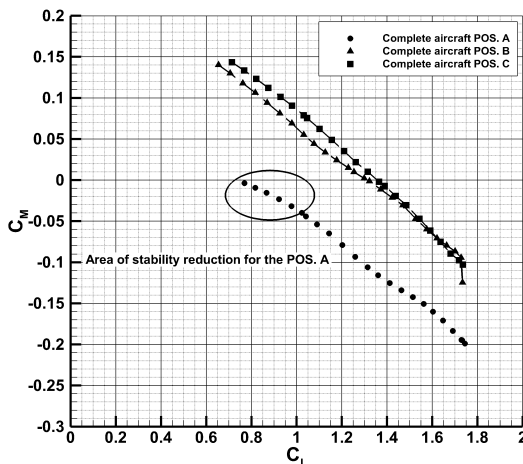


Figure 10: Effect of vertical positioning of the horizontal tail, pitching moment coefficient, Flap = 40°,  $x_{cg}/c=0.25$   $z_{cg}/c = 0.25$   $i_{to} = 0^\circ$

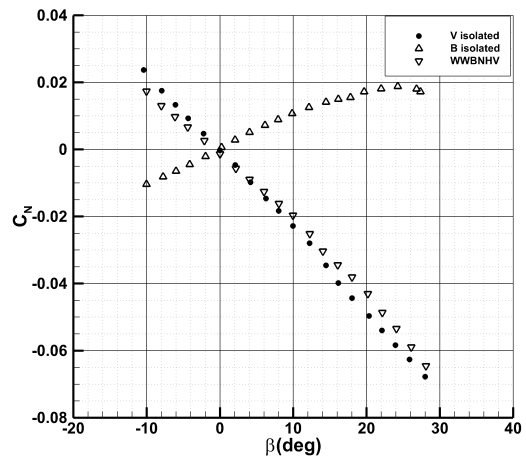


Figure 11 – Yawing moment breakdown.

The complete aircraft shows a  $C_{N\beta}$  of about  $-0.00184 \text{deg}^{-1}$ .

In order to estimate the aircraft lateral control capabilities the complete aircraft at several rudder deflections has been tested.

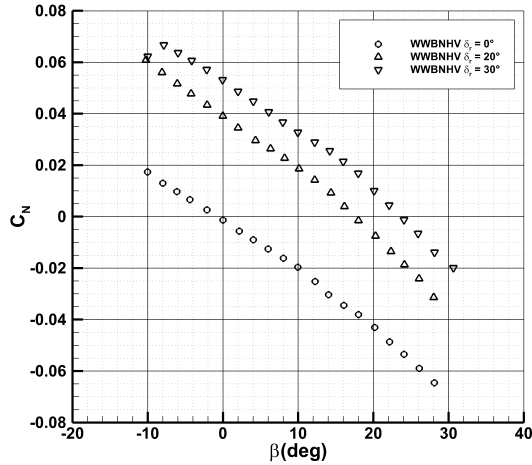


Figure 12 – Yawing moment coefficient of complete aircraft with different rudder deflections.

Figure 12 show yawing moment coefficient variation for several rudder deflections. The complete aircraft has shown a control power of about  $0.0020 \text{deg}^{-1}$ .

Figure 13 shows the rolling moment coefficient respect to the sideslip angle. The complete aircraft shows a lateral stability derivative (dihedral effect) of about  $-0.0030 \text{deg}^{-1}$ . A relevant result is the estimation of the winglet contribution to the lateral stability characteristic. As matter of fact the introduction of the winglet leads to a wing dihedral effect 36% more than the winglet-off configuration, as it is highlighted in Figure 13.

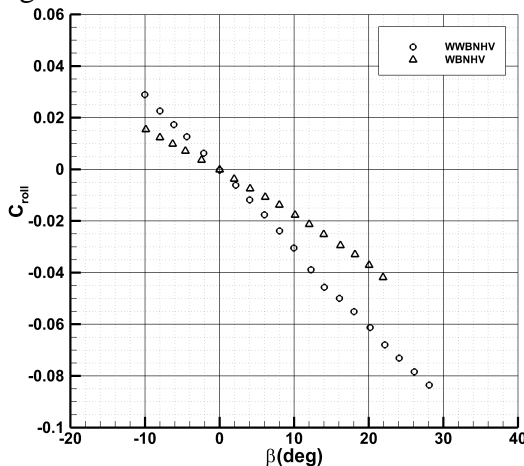


Figure 13 – Rolling moment coefficient vs sideslip angle (dihedral effect), complete aircraft with and without winglet.

### 3 CFD Navier-Stokes aerodynamic analyses

The CAE package Star-CCM+ [21] has been used for the CFD Navier-Stokes simulations,

which have been executed on the University’s grid computing infrastructure ScoPE [20] to perform parallel computations up to 128 CPUs for each run.

The 3D model of the aircraft has been imported from external CAD software and divided into main aircraft components (wing-body-nacelle-horizontal-vertical tail-flap etc.), as shown in Figure 14. A parallelepiped box has been created to simulate the fluid region which dimensions are shown in Figure 15 in terms of wing span.

Polyhedral mesh with prismatic layers has been used in all the CFD simulations (see Figure 16 and Figure 17). The flow field has been imposed to be steady, subsonic, compressible, and fully turbulent with Spalart-Allmaras model, demonstrated to be reliable at this flow condition [19][22][23].

Velocity inlet and pressure outlet boundary conditions have been imposed at the inflow and outflow zone respectively.

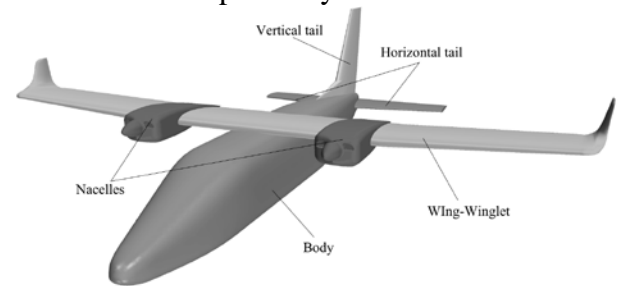


Figure 14 – P2012 Components into CFD analyses.

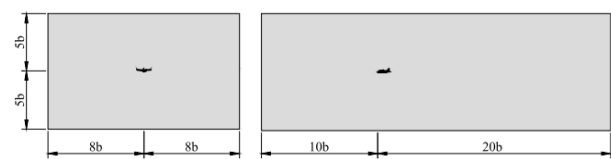


Figure 15 – Parallelepiped box size in span length b.



Figure 16 – Complete aircraft polyhedral mesh.

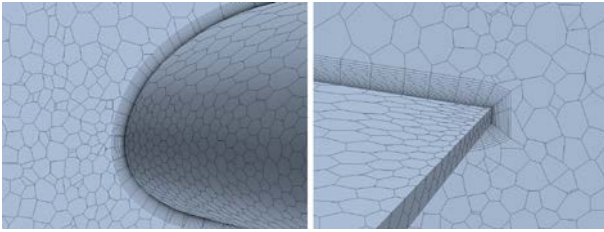


Figure 17 – Prismatic layer on wing leading and trailing edges

Mesh independence from number of cells, solution convergence and boundary layer phenomena ( $y^+ \approx 1$ ) have been obtained, performing an accurate meshing set-up (at different Reynolds number).

Mesh details and physics settings are summarized in Table 5. Wind-tunnel, cruise and take-off and landing Mach and Reynolds number conditions have been investigated, re-meshing opportunely the volume of fluid. Longitudinal aerodynamic analyses have been performed on the semi-model (with and without flaps), while lateral directional analyses have been carried out on the complete model. Results are summarized in sections 3.1 and 3.2 respectively.

### 3.1 CFD Longitudinal aerodynamic analyses

Longitudinal Navier-Stokes aerodynamic analyses have been performed on several aircraft configurations. In this section complete aircraft, flaps effects, horizontal tail position effects, wing span loading and drag coefficient breakdown will be shown, also with some details on Reynolds number effects.

Property	Value
Complete Aircraft	8.5 e6 cells
Take-off and Landing	11.5 e6 cells
Complete Lateral-directional	15.1 e6 cells
Prismatic layers	20
Near wall cell Re 0.6e6	0.5 e-4 m
Near wall cell Re 4.5e6	2e-6 m
Near wall cell Re 9.5e6	1e-6 m
Turbulent model	S-A
$M_{(WT, T-O, LNG)}$	0.12
$M_{cruise}$	0.23
$X_{cg}, Z_{cg}$	$0.25 \bar{c}, 0.25 \bar{c}$

Table 5 – Mesh details and physics settings.

#### 3.1.1 Complete aircraft in clean, take-off and landing configurations

Figure 18 shows the complete aircraft lift coefficient in clean, take-off and landing conditions. As it can be seen a very good agreement between numerical and experimental data in clean condition is visible both in  $CL_0$  and  $CL_\alpha$ . In flapped configuration there is a good agreement in terms of lift curve slope while the numerical approach overestimates the  $C_{L0}$ . This fact can be due to two main reasons: 1<sup>st</sup> the uncertainty of wind-tunnel flap deflection measured by hand. 2<sup>nd</sup> the very little flap geometry, gap and overlap can lead to a choked channel due to the very low local Reynolds number. Wind-tunnel and free flight Reynolds numbers are also compared in clean configuration and the effect is visible only at stall condition where maximum lift coefficient is increased of about 0.2.

Numerical and experimental pitching moment coefficients are compared in Figure 19. Longitudinal stability is in good agreement in clean and flap equal to 15°. Numerical analyses overestimate the pitching moment curve in landing configuration. However stability reduction (at low attitude) due to the flap deflections can be also highlighted in CFD analyses.

Figure 20 shows drag polar comparison. It is evident that CFD underestimates  $C_D$  in clean configuration, well predicts  $C_D$  at flap 15° and slightly overestimates at flap 40°.

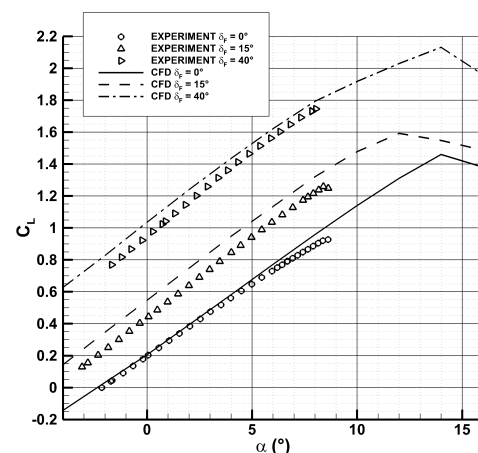


Figure 18 – Complete Aircraft lift coefficient,  $Re=0.6e6$

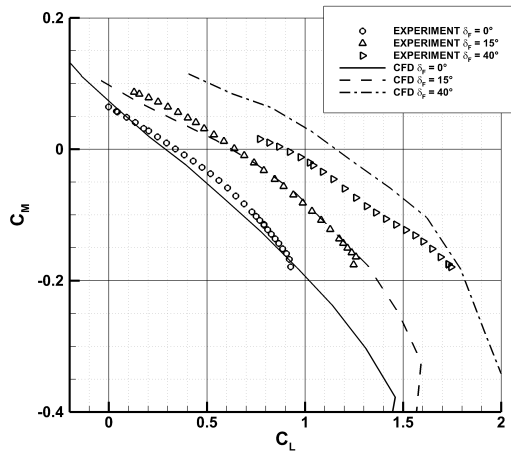


Figure 19 – Complete Aircraft pitching moment coefficient, Re=0.6e6, cruise condition

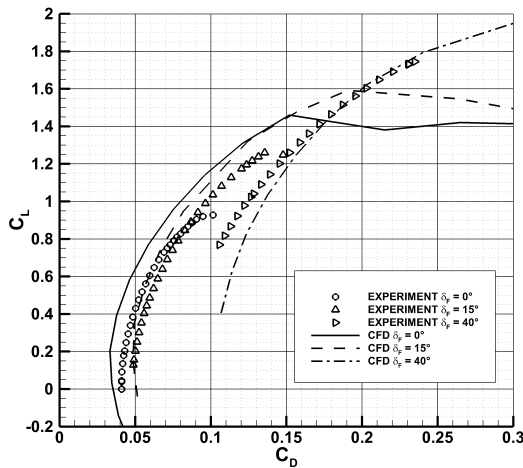


Figure 20 – Complete Aircraft drag coefficient, Re=0.6e6

3.1.2 Horizontal tail position analyses

The horizontal tail vertical position has been also analyzed through numerical CFD aerodynamic analyses at the three flap condition to better understand wake and downwash effects. Results are shown in clean condition (see Figure 21) and summarized for all condition in Table 6. As clearly outlined in Figure 21 both experimental and CFD analyses show a sensible stability reduction at typical cruise attitude ( $C_L = 0.4-0.6$ ) for POS. B and POS. C.

How well explained in section 2.1.2, the position A has a reduction in terms of stability in full flap condition (see Table 6). In Figure 22 the off-body streamlines at zero angle of attack and flap deflected in take-off condition (15 deg.) for position A and B of the horizontal tail are depicted. Increasing the angle of attack, for the POS. B and POS. C, the wing wake goes

through the horizontal tail (from the bottom to the top side of the tail), decreasing the longitudinal stability, as shown in Table 6.

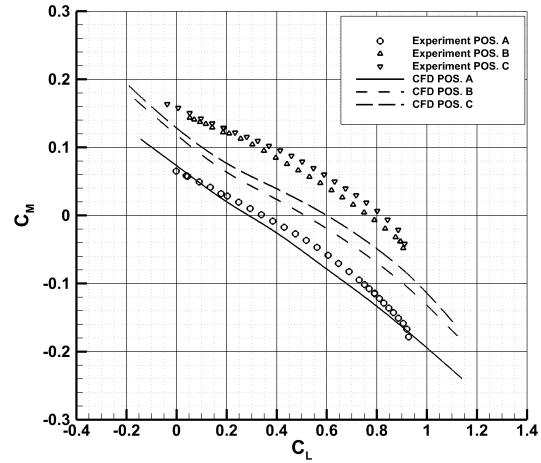


Figure 21 – Horizontal tail position, CFD vs. Wind-Tunnel, Re=0.6e6, cruise condition (flap=0 deg.)

CONFIGURATION	$N_0$ (%CMA)		
	POS. A	POS.B	POS.C
FLAP = 0°			
$C_L$ [0.2; 0.6]	49.0	45.6	44.1
FLAP = 15°			
$C_L$ [0.6; 1.2]	51.0	41.1	46.8
FLAP = 40°			
$C_L$ [1.2; 1.7]	46.2	42.9	47.2

Table 6 - Effect of vertical position of the horizontal plane, CFD analysis, Re=0.6e6

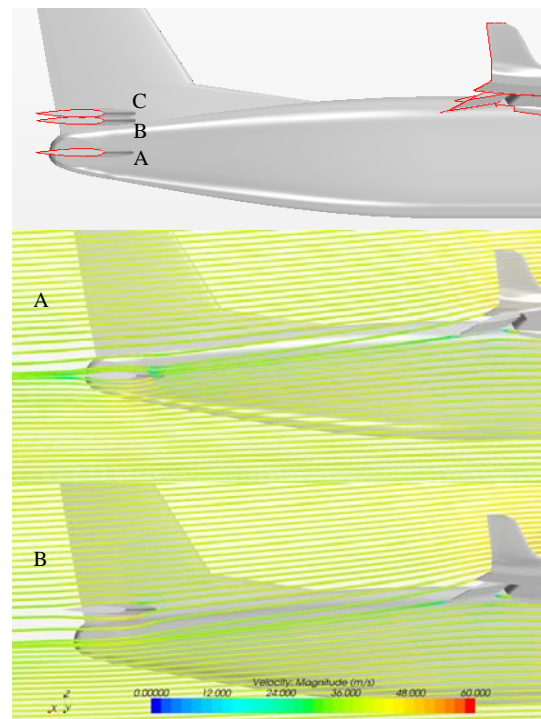


Figure 22 – Off body streamlines, aoa=0deg., flap 15deg., Re=0.6e6

### 3.1.3 Wing span loading analyses

Navier-Stokes aerodynamic analyses have been very useful to evaluate the aircraft wing span loading and the aircraft stall path. The former is crucial to dimension the wing box structure, the latter is very important to understand the aircraft stall quality. Several wing and nacelle slice sections have been extracted from Navier-Stokes analyses for both clean and flapped configurations as shown in Figure 23. Pressure and friction section distributions have been opportunely integrated to evaluate the wing span loading and the fuselage contribution (dimensionless on the wing root chord). Clean and landing stall path and wing span loading are shown in Figure 24 and Figure 25 respectively.

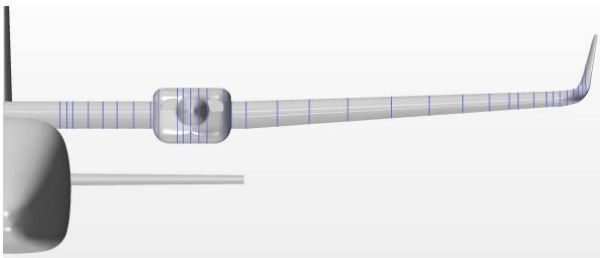


Figure 23 – Sections extracted from aerodynamic analyses.

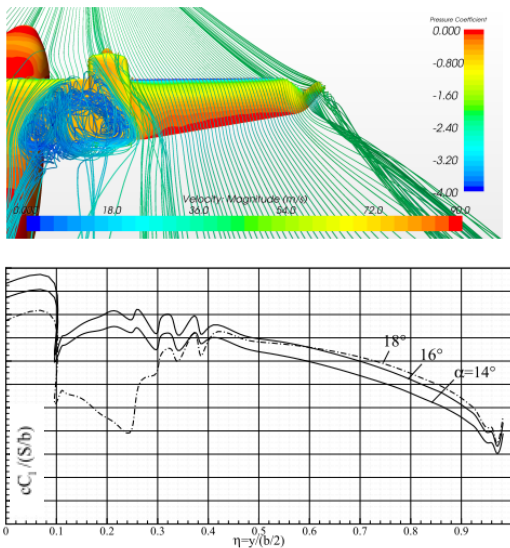


Figure 24 – Clean condition stall path and wing span loading  $Re=9.5e6$ .

As it can be seen the stall path is similar for both clean and flapped configurations. The abrupt lift coefficient reductions start from the inner wing zone (across fuselage and nacelle zone). This behavior is desirable because avoid the loss of aileron control and an abrupt rolling

moment. The velocity off body streamlines well show the vortices separation zone. In clean condition (Figure 24) at  $\alpha=18^\circ$  the flow separates from the inner wing zone causing vortices which curve the flow along spanwise direction (see on the nacelle zone). The same behavior can be seen in Figure 25 when flaps are extended.

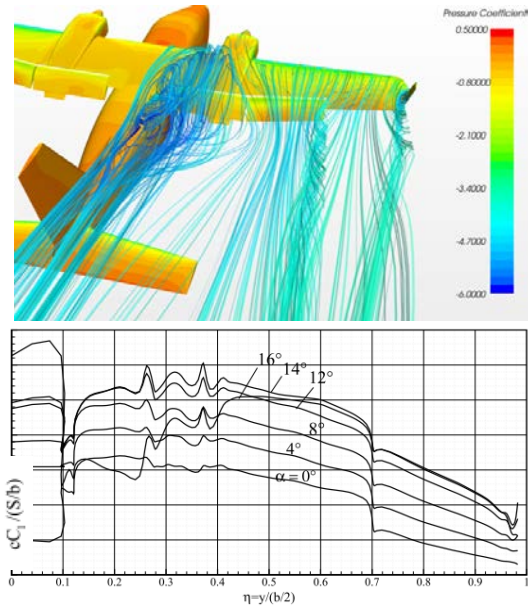


Figure 25 – Landing condition stall path and wing span loading  $Re=4.5e6$ .

### 3.1.4 Drag breakdown

Zero lift drag coefficient breakdown has been evaluated at wind-tunnel Reynolds number and free flight Reynolds number. Results are shown in Figure 26 and Figure 27.

$C_{D0}$  resulted equal to 345 drag counts in wind-tunnel Reynolds number and 239 drag counts at Reynolds equal to  $9.5e6$ . As it can be seen the drag contributions are almost equally divided among wing, fuselage and nacelles components (30%, 30%, 30%) and 10% to the tailplanes. It is interesting to notice the high value of nacelles component of about 30% of total  $C_{D0}$ . In particular this contribution is divided about 80% in pressure and 20% in friction contributions.

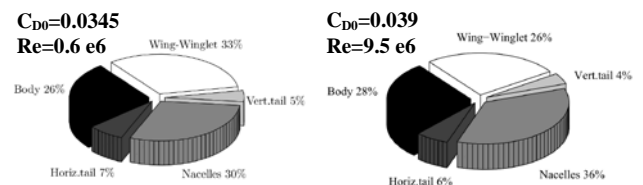


Figure 26 – Pie charts of  $C_{D0}$  percentage contributions.

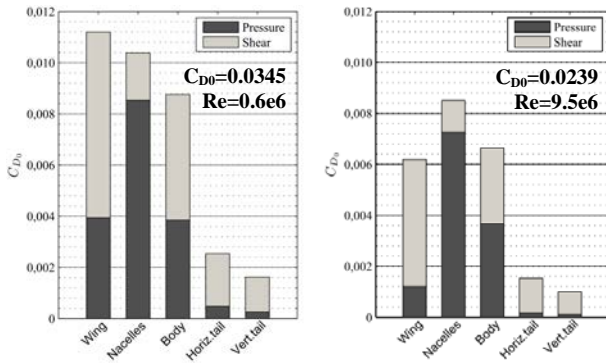


Figure 27 – Components  $C_{D0}$  pressure and friction contributions.

This effect is from one hand due to the mid wing nacelle, leading edge and trailing edge nacelle geometry, and from the other hand due to an erroneous CFD simulation of the inflow and exhaust nacelle boundary conditions supposed simply closed in the present aerodynamic analyses (see Figure 28). Flow stagnation in the front and rear zone are clearly visible from the velocity streamlines of Figure 28.

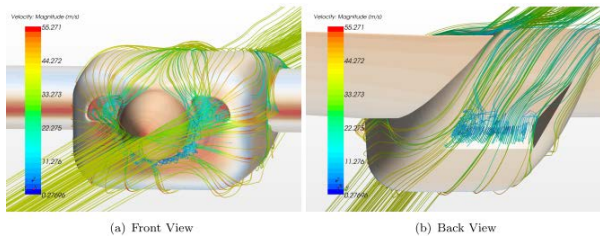


Figure 28 – Nacelle off-body streamlines,  $C_L=0.0$ .

### 3.2 CFD Lateral-Directional aerodynamic analyses

The lateral directional Navier-Stokes aerodynamic analyses have been performed on the complete model. Results on complete aircraft and winglet effects on lateral stability are here presented.

#### 3.2.1 Complete aircraft Directional analyses

Directional results of complete aircraft are shown in Figure 29 compared to experimental results. Reynolds number effect and aircraft components contributions to the lateral-directional stability are in Table 7 and Table 8 respectively.

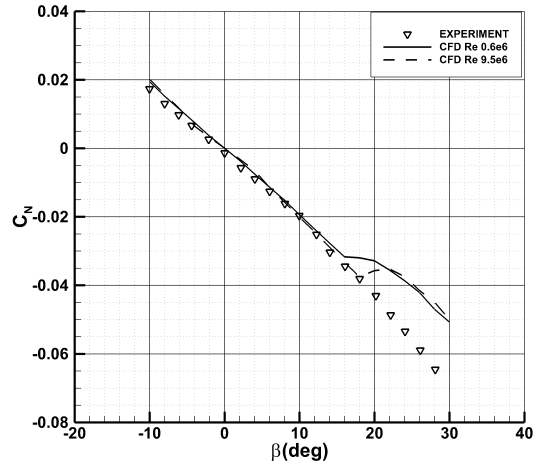


Figure 29 – Complete aircraft yawing moment coefficient.

Reynolds Number	$C_{Y\beta}$ 1/deg.	$C_{N\beta}$ 1/deg.	$C_{roll\beta}$ 1/deg.
0.6e6	-0.0131	-0.00183	-0.00254
9.5e6	-0.0133	-0.00203	-0.00256

Table 7 – Reynolds number effect to the lateral-directional derivatives.

Components	$C_{Y\beta}$ 1/deg.	$C_{N\beta}$ 1/deg.	$C_{roll\beta}$ 1/deg.
Vertical	-0.00711	-0.00274	-0.00067
Fuselage	-0.00394	0.00087	0.00015
Wing-wlet	-0.00172	0.00001	-0.00216
Nacelle	-0.00010	0.00004	-0.00019
Horizontal	-0.00002	0.00000	0.00035
Total with winglet	-0.01310	-0.00183	-0.00254
Total			
No winglet	-0.01180	-0.00173	-0.00154

Table 8 – Aircraft components contributions to the lateral-directional derivatives.

Looking at Figure 29, yawing moment coefficient is in very good agreement between wind-tunnel and CFD aerodynamic analysis until a sideslip angle equal to  $\beta=18^\circ$ . At this sideslip angle the flow tends to separate at the outer zone of the vertical tail (see Figure 30) while in the inner zone of the vertical tail the dorsal fin vortices allow the flow to remain attached as shown in Figure 30. Table 7 and Table 8 show a little effect of both Reynolds number and winglet on the directional stability (about 6%).

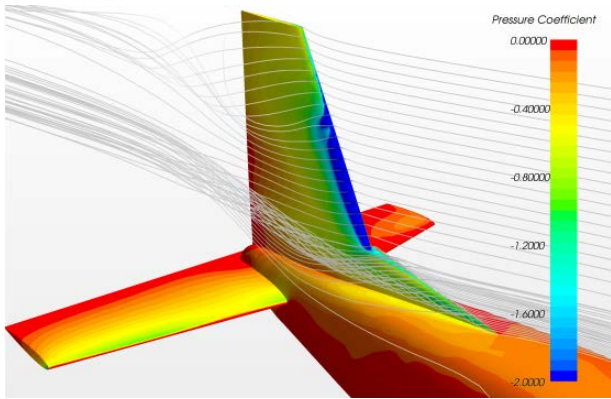


Figure 30 – Complete aircraft in sideslip, effect of dorsal fin vortices,  $\beta=20^\circ$ ,  $Re=0.6e6$ .

### 3.2.2 Complete aircraft Lateral analyses

Lateral stability curve  $C_{Y\beta}$  is shown in Figure 31 with and without winglet, compared to wind-tunnel results. Numerical analyses slightly underestimate the dihedral effect both with and without winglets. The winglet effect on lateral moment coefficient is well predicted also in the CFD analyses, increasing of about 35% with winglet. The difference between numerical CFD values and experimental ones is mainly due to the small difference in wing dihedral between the two models. The model used for wind-tunnel tests has been built with a certain degree of accuracy (it is not completely machined) and the wing dihedral angles (that could also be slightly different for right and left wings) are not possible to be measured accurately. This leads to a small difference in wing dihedral from CFD model (where the wing dihedral is fixed as in aircraft CAD drawing).

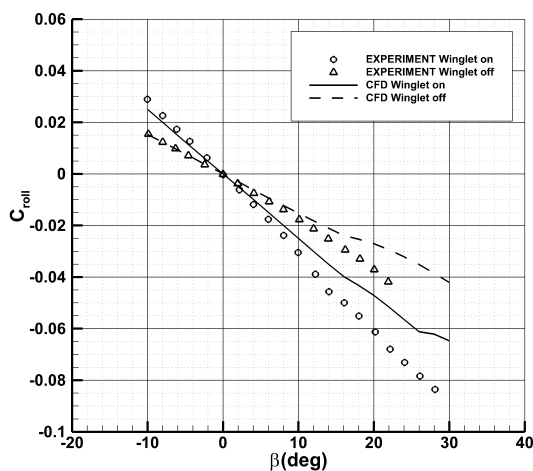


Figure 31 – Complete aircraft rolling moment coefficient with and without winglet.

## References

- [1] Giordano V., Coiro D.P., Nicolosi F. Reconnaissance Very Light Aircraft Design. Wind-Tunnel and Numerical Investigation, *Engineering Mechanics*, Vol. 7, No. 2, pp. 93-107, 2000. ISSN 1210-2717.
- [2] Coiro D.P., Nicolosi F. Aircraft Design through Numerical and Experimental Techniques Developed at DPA, *Aircraft Design Journal*, Vol. 4, No. 1, March 2001, ISSN 1369-8869.
- [3] Coiro D.P. and Nicolosi F. Design of a Three Surfaces R/C Aircraft Model, *Acta Polytechnica*, Vol. 42, No. 1, 2002, pp. 44-52, ISSN 1210-2709.
- [4] Coiro D.P., Nicolosi F., De Marco A., Genito N. and Figliolia S. Design of a Low Cost Easy-to-Fly STOL Ultralight Aircraft In Composite Material, *Acta Polytechnica*, Vol. 45, No. 4, 2005, pp. 73-80, ISSN 1210-2709.
- [5] Coiro D.P., Nicolosi F., Grasso F. Design and Testing of Multi-Element Airfoil for Short-Takeoff-and-Landing Ultralight Aircraft, *Journal of Aircraft*, Vol. 46, No 5, pp. 1795-1807, ISSN 0021-8669, doi: 10.2514/1.43429.
- [6] Pascale, L. and Nicolosi, F. Design and aerodynamic analysis of a twin engine propeller aircraft, *26<sup>th</sup> ICAS conference*, Anchorage (Alaska, US), 14-19 September, 2008, ISBN 0-9533991-9-2.
- [7] Nicolosi F., De Marco A., Della Vecchia P. Flight Tests, Performances, and Flight Certification of a Twin-Engine Light Aircraft, *Journal of Aircraft*, Vol. 48, No.1, 2011, pp. 177-192. ISSN 0021-8669, doi: 10.2514/1.C031056.
- [8] Nicolosi, F., De Marco, A. and Della Vecchia, P. Stability, flying qualities and longitudinal parameter estimation of a twin-engine CS-23 certified light aircraft, *Aerospace Science and Technology*, Vol. 24, No 1, pp. 226-240, doi: 10.1016/j.ast.2011.11.01, Scopus eid code:2-s2.0-84875514126.
- [9] Nicolosi, F., Della Vecchia, P. and Corcione, S. Aerodynamic analysis and Design of a twin engine commuter aircraft, *28th ICAS Conference*, Brisbane (Australia) 23-28 September 2012, ISBN: 9780956533319.
- [10] Corcione S. and Nicolosi F. Wind Tunnel Tests of a New Commuter Aircraft, *22th AIDAA Conference*, Napoli (Italy), Paper 128, 2013.
- [11] Barlow J.B., RAE W.H., POPE A., *Low-speed wind tunnel testing*, 1984, John Wiley & Sons, Inc.
- [12] Silvertain A., Katzoff, Design charts for predicting downwash angles and wing wake characteristics behind plain and flapped wings, NACA REPORT No. 648.
- [13] Corcione S., Nicolosi F., Della Vecchia P. Wind Tunnel Tests of a New Commuter Aircraft, *4th CEAS Conference*, ISBN: 978-91-7519-519-3, 16-19 September 2013, Linkoping (Sweden), pp. 138-149.
- [14] Zhang M., Rizzi A., Nicolosi F., De Marco A. Collaborative Aircraft Design Methodology using ADAS Linked to CEASIOM, *32<sup>nd</sup> AIAA Applied Aerodynamics Conference*, doi:10.2514/6.2014-2012.

- [15] Della Vecchia P., Development of Methodologies for the Aerodynamic Design and Optimization of New Regional Turboprop Aircraft, Doctoral Thesis in Aerospace, Naval and Quality Engineering, University of Naples, ISBN 978-88-98382-02-6.
- [16] Nicolosi F, Della Vecchia P and Ciliberti D. An investigation on vertical tailplane contribution to aircraft sideforce, *Aerospace Science and Technology*, Vol. 28, pp. 401-416, 2013, doi: 10.1016/j.ast.2012.12.006, Scopus eid code: 2-s2.0-84878839559.
- [17] Nicolosi F, Della Vecchia P and Ciliberti D. Aerodynamic interference issues in aircraft directional control. *Journal of Aerospace Engineering*, 2014, ISSN 0893-1321, doi: 10.1061/(ASCE)AS.1943-5525.0000379, 04014048
- [18] Ciliberti D, Nicolosi F and Della Vecchia P. A new approach in aircraft vertical tailplane design, *22th AIDAA Conference*, Napoli (Italy), Paper 034, 2013.
- [19] Della Vecchia P., Ciliberti D. Numerical aerodynamic analysis on a trapezoidal wing with high lift devices: a comparison with experimental data, *XXII AIDAA Conference*, ISBN: 978-88-9064842-7, 9-12 September 2013, Naples (Italy).
- [20] SCoPE, Università degli studi di Napoli "Federico II", <http://scope.unina.it/>, 2012.
- [21] Star-CCM+ Version 8.04.007-R8 User Guide, CD-adapco, 2013.
- [22] Antunes A P, da Silva R G, Luiz J and Azevedo F. On the effects of turbulence modeling and grid refinement on high lift configuration aerodynamic simulations. in: *28th ICAS Congress*, Brisbane (Australia), 2012.
- [23] Rumsey C L, Long M, Stuever R A and Wayman T R. *Summary of the First AIAA CFD High Lift Prediction Workshop*. AIAA-2011-839, American Institute of Aeronautics and Astronautics, 2011.

### Copyright Statement

The authors confirm that they, and/or their company or organization, hold copyright on all of the original material included in this paper. The authors also confirm that they have obtained permission, from the copyright holder of any third party material included in this paper, to publish it as part of their paper. The authors confirm that they give permission, or have obtained permission from the copyright holder of this paper, for the publication and distribution of this paper as part of the ICAS 2014 proceedings or as individual off-prints from the proceedings.